Available online at www.sciencedirect.com
SCIENCE DIRECT®
ELSEVIER
Earth and Planetary Science Letters 213 (2003) 347–359
EPSL
www.elsevier.com/locate/epsl

How do asperities fracture? An experimental study of unbroken asperities

Xinglin Lei [a,b]

[a] *Experimental Earthquake Physics Research Group, Institute of Geoscience, Geological Survey of Japan, AIST, 1-1-7 Higashi, Tsukuba City, 305-8567 Ibaraki-ken, Japan*
[b] *Institute of Geology and Laboratory of Tectonophysics, China Seismological Bureau, Beijing, PR China*

Received 12 February 2003; received in revised form 22 May 2003; accepted 12 June 2003

Abstract

The fracture of a shear fault containing several unbroken asperities in a granitic porphyry is examined in detail via acoustic emission (AE) data collected by a high-speed multi-channel waveform recording system. The experimental results reveal that a quasi-static nucleation of the shear faulting corresponds to the fracture of coupled asperities on the fault plan. AEs caused by the fracture of individual asperities exhibit similar characteristics to the sequence for natural earthquakes, including foreshock, mainshock, and aftershock events. Foreshocks, initiated at the edge of the asperity, occur with an event rate that increases according to a power law of the temporal distance to the mainshock, and with a decreasing *b*-value (from $\sim$1.1 to $\sim$0.5). One or a few mainshocks then initiate at the edge of the asperity or the front of the foreshocks. The aftershock period is characterized by a remarkable increase and subsequent gradual decrease in *b*-value and a decreasing event rate obeying the modified Omori law, which has been well established for earthquakes. The fracture of neighboring asperities is then initiated after the mainshock of a particular asperity, presumably due to redistribution of the strain energy accumulated within an asperity, which is released by the mainshock, resulting in enhancement of the stress concentration around the nearest neighboring intact asperities. The progressive fracturing of multiple, coupled asperities during the nucleation of shear faulting results in short-term precursory fluctuations in both *b*-value and event rate, which may prove useful information in the prediction of failure of the main fault plane of seismic earthquakes.

Keywords: asperity; fault nucleation; acoustic emission; *b*-value; Omori's law; foreshock; aftershock

1. Introduction

The word 'asperity' originally denoted a region of contact between two flat load-bearing surfaces, but is frequently used in seismology following Kanamori and Stewart [1] to indicate a patch on a fault surface offering greater than average resistance to rupture and releasing larger seismic moment during a subsequent earthquake. Seismologists also use the word 'barrier', after Aki [2,3], to indicate a region of fault surface or the extension of a fault plane that arrests seismic rupture. A barrier can be broken during an earthquake and will exhibit similar behavior to an asperity. An asperity can also arrest fault rupture in a similar

E-mail address: xinglin-lei@aist.go.jp (X. Lei).

0012-821X/03/$ – see front matter © 2003 Elsevier B.V. All rights reserved.
doi:10.1016/S0012-821X(03)00328-5

manner to a barrier. Hence, the word 'barrier' should be used only when it plays a role in arresting earthquake rupture, otherwise, 'asperity' is a better term. A fault plane can be expected to incorporate various types of asperities at all scales, including heterogeneous contacts between two rough fault surfaces, unbroken patches of a fault plane within an otherwise ruptured region, and locked regions in a creeping segment due to inhomogeneities in permeability and core pressure, for example. In all cases, the regions surrounding an asperity rupture more readily than the asperity itself, and under tectonic loading more strain energy accumulates at the asperity. In addition, once an asperity does rupture, more seismic energy is radiated from it than from the surrounding areas. The adjacent (non-asperity) surface may slip slowly and continuously, and exhibit creeping or ductile features.

Many recent studies of near-field strong motion records have revealed that not only large earthquakes of $M > 6$ (e.g. [4–6]) but also moderate earthquakes of $M \approx 4$–5 (e.g. [7,8]) have complex coseismic slip distributions on the seismic fault, indicating complex distributions of asperities. At present, there is also no evidence to suggest that faulting complexity is related to fault size. Asperities play an important role in the generation of high-amplitude seismic waves and may control the localities of foreshocks, mainshocks and aftershocks. Many large earthquakes appear to be located at the edge of major asperities in seismically active areas such as the Kanto area of Japan [9] and the Pacific coast of Mexico [10]. In many cases, large aftershocks and foreshocks have occurred outside the main asperity (e.g. [11]). It has also been recognized that small isolated asperities surrounded by an otherwise creeping fault plane may lead to repeating sequences of earthquakes [12–14]. Smaller asperities at a boundary between large locked and creeping fault patches are presumed to represent the sources of repeating earthquakes of low stress drops [14].

Understanding the fracturing characteristics of individual asperities, as well as multiple, coupled asperities on a fault plane, is important for elucidating the physics of the initial fracturing process and may make it possible to obtain accurate short-term predictions for large earthquakes and large associated aftershocks. The final dynamic fracture process of asperities has been studied through waveform inversion and numerical simulation [15]. However, the detailed process, particularly in the early stage of asperity fracture, and the role of asperities in fault nucleation remain poorly understood. Furthermore, asperities estimated from seismic waveform inversion indicated regions that had released larger seismic moment during a past earthquake, and it is unclear why such regions remain stronger than the surrounding areas.

Laboratory studies under well-controlled conditions, using well-prepared samples containing well-known asperities are expected to be useful for understanding the physics of asperities. In recent years, experiments employing acoustic emission (AE) technology have established remarkable results concerning quasi-static fault growth (e.g. [16]), the model of the process zone [17,18], and the role of pre-existing density of microcracks and strong asperities in the faulting process [19,20]. Such experiment-based knowledge is expected to be useful for studying the fundamental behavior of natural earthquakes because it is widely accepted that fault systems are scale-invariant [21–23] and there exist universal similarities between faulting behaviors, from small-scale microcracking to large-scale seismic faulting. For example, AE events caused by microcracking activity (e.g. [16–20,24]) and stick-slip along a fault plane [25] are similar to those generated by natural earthquakes, indicating similarity in terms of the focal mechanism (e.g. [17]), frequency–magnitude distribution [24], and fractal structure of hypocenter distributions (e.g. [26]). More recently, Lei et al. [27] presented experimental results illustrating the hierarchical fracture process of a heterogeneous shear fault and suggested that those experimental results may guide future studies on earthquakes. As a continuation of this theme, the goal of the present study was to employ AE measurements to establish how an individual asperity fractures, how coupled asperities fracture, and the role of asperities in fault nucleation and as potential precursors prior to dynamic rupture. Based on the experimental results obtained in this study, a

new similarity between the fracture of asperities in laboratory-scale experiments and tectonic-scale events is suggested. AE data for laboratory-scale experiments exhibit an analogous sequence to natural earthquakes, including foreshock, the mainshock and aftershocks. Although there remain significant problems in extrapolating laboratory results to natural conditions, experimental results may still provide a basis for modeling the poorly understood final phase of faulting nucleation prior to large earthquakes.

2. Experiment and data

A detailed description of the test sample, identification of asperities on the fault plane, experimental setup, and the AE data processing procedure can be found in Lei et al. [27]. The test sample is cylindrical, with a diameter of 50 mm and a length of 100 mm. As illustrated in Fig. 1, the sample contains a pre-existing, naturally healed joint with discontinuities and bends. The experiment was carried out under tri-axial compression conditions ($\sigma_2 = \sigma_3$). The sample was loaded step-wise to 850 MPa, at which point the axial stress was maintained constant. The confining pressure (oil) was maintained constant at 60 MPa throughout the test. A shear fault formed along part of the pre-existing joint, which was presumably weaker than the adjacent host rock. The fault contained six recognizable first-order geometric/mechanical asperities, which were identified based on the geometric relationship between the fault surface and the pre-existing joint, and microscopic observations of the fault surface after the test. The discontinuities along the joint were easy to identify after the test because the joint was apparent as a thin darker layer in the lighter host rock. Although AE hypocenters were not used to identify asperities, the AE events concentrated in dense clusters around the identified asperities, demonstrating that AE hypocenters can also be used to identify asperities if necessary. Fig. 1b shows the locations of asperities on the fault plane. Asperity 1 corresponds to an originally strongly healed region along the original joint, and asperities 2–5 are located at discontinuities

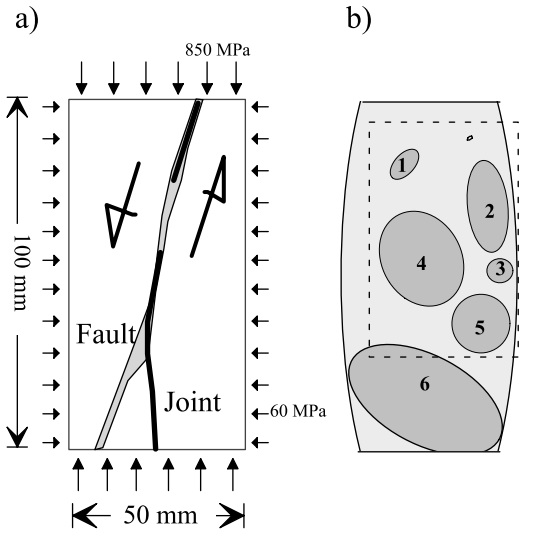

Fig. 1. (a) Test sample and (b) major asperities on the fault surface produced during loading. The sample contains a pre-existing naturally healed joint with discontinuities and bends. The shear plane developed along part of this joint, and is considered to be analogous to a natural fault containing strong intact asperities. Six recognizable first-order asperities (1–6) are located along the fault surface.

in the joint. Asperity 6 is located at the point where the fault diverges from the joint due to the bend in the joint within the lower half of the sample. These asperities fractured during the initial fracture process preceding dynamic fracture of the principal shear fault. Hence, this experiment may constitute a good mechanical analogue for natural earthquake faults with complex structures under steady tectonic loading.

As seen from Fig. 1, the fault ruptured towards the end caps. Mechanically, the end caps play the role of strong barriers that arrest the rupture of the fault, and thus make the experimental configuration more complicated. Since a natural fault has a limited length and intersects the host rocks at the ends of the fault, the boundary condition in the present experiment does not change the effectiveness of the test. Furthermore, all asperities mentioned above fractured during the quasi-static nucleation stage of the fault (see Section 3 for details). At this stage, the shear displacement of the fault and dilatancy of the sample as a whole

are very limited. Hence, the effect of the end caps is not a significant factor in the fracturing process of asperities. The boundary condition may impart strong control on the dynamic rupture of the fault, but that is beyond the scope of this paper.

During the experiment, the data recording system recorded maximum amplitudes of more than 30 000 AE events. A two-channel peak detector with an effective dynamic range of 55 dB was used to record the maximum amplitudes at two sensors mounted on the central surface of the sample. Of these events, the waveforms of the ~10 000 largest were recorded at 32 piezoelectric transducers sensors mounted on the surface of the sample. Waveforms were digitized with a dynamic range of 12 bits and a sampling rate of 20 MHz. Two waveforms from the sensors connected to the peak detector were also digitized at 10 MHz by an independent recorder with wide dynamic range (16 bits) and long sampling length (selectable between 100 μs and 1 s). Long-waveform data were used to estimate the magnitude of some very large events (mainshocks associated with the fracture of the asperities), which saturated the peak detector. About 8000 hypocenters were determined precisely using the first arrival times at the 32 sensors and P-velocities measured along multiple paths during the experiment. Location errors are estimated to be less than 2 mm in most cases, as determined by numerical simulation [28] and AE data for several samples of ductile mudstone containing brittle quartz veins of 1–3 mm thickness. In these mudstone samples, almost all AEs occurred along the intersections of the veins and the ultimate fault plane, which formed along the bedding plane of the mudstone. The AE hypocenters are coincident with veins, with a statistical location error of less than 2 mm [20].

A relative magnitude was calculated from the maximum amplitude data according to the relation:

$$M = \log(A_{\max}/A_0) \quad (1)$$

where $A_{\max}$ is the maximum amplitude and A_0 is the threshold for detection. The effective dynamic range of 55 dB as mentioned above results in a magnitude range of 2.75. The b-value in the magnitude–frequency relation was calculated by the maximum likelihood technique for a running window of 500/100 events with a step of 125/25.

The AE data revealed three distinct stages of microcrack activity during deformation and faulting of the sample, referred to as the primary, secondary and nucleation stages [27]. In the primary and secondary stages, AE hypocenters are distributed throughout the entire sample and form clusters with a dimension comparable to the average grain size of ~7 mm. In the primary stage, b-values increase with time from ~0.8 to ~1.2, and decrease during the secondary stage from ~1.2 to ~1.0. The third stage corresponds to the initiation and quasi-static nucleation of the principal shear fault, and is referred to as the nucleation stage. The nucleation stage, in which asperity fracture occurs, is the focus of this paper.

3. Fracture of asperities

Fig. 2 shows the basic AE results for the nucleation stage. Approximately 25 000 AE events were detected, and 4500 hypocenters were determined. The duration of the nucleation stage is only ~20 s. During this period, axial stress and confining pressure were maintained constant at 850 MPa and 60 MPa, respectively. The b-values plotted in Fig. 2a were calculated by the maximum likelihood technique for a running window of 500 events with a step of 125. The b-values vary between 0.5 and 1.3, in agreement with observations along fault zones [29]. Correlated fluctuations of large amplitude in AE rate and b-value were observed. Each main peak in the AE rate corresponds to a minimum in the b-value. AE hypocenters were generally confined to the fault plane and formed several dense clusters within the asperities shown in Fig. 1b. It is clear that each cluster corresponds to a peak in the AE rate or minimum in the b-value. AE hypocenters migrated with a velocity of 0.8 cm/s, resulting in a moving process zone (Fig. 2d). This demonstrates that the initial fracturing, or quasi-static nucleation, of the shear fault corresponds to progressive fracture of coupled asperities on the incipient fault surface.

The AE events associated with the fracture of

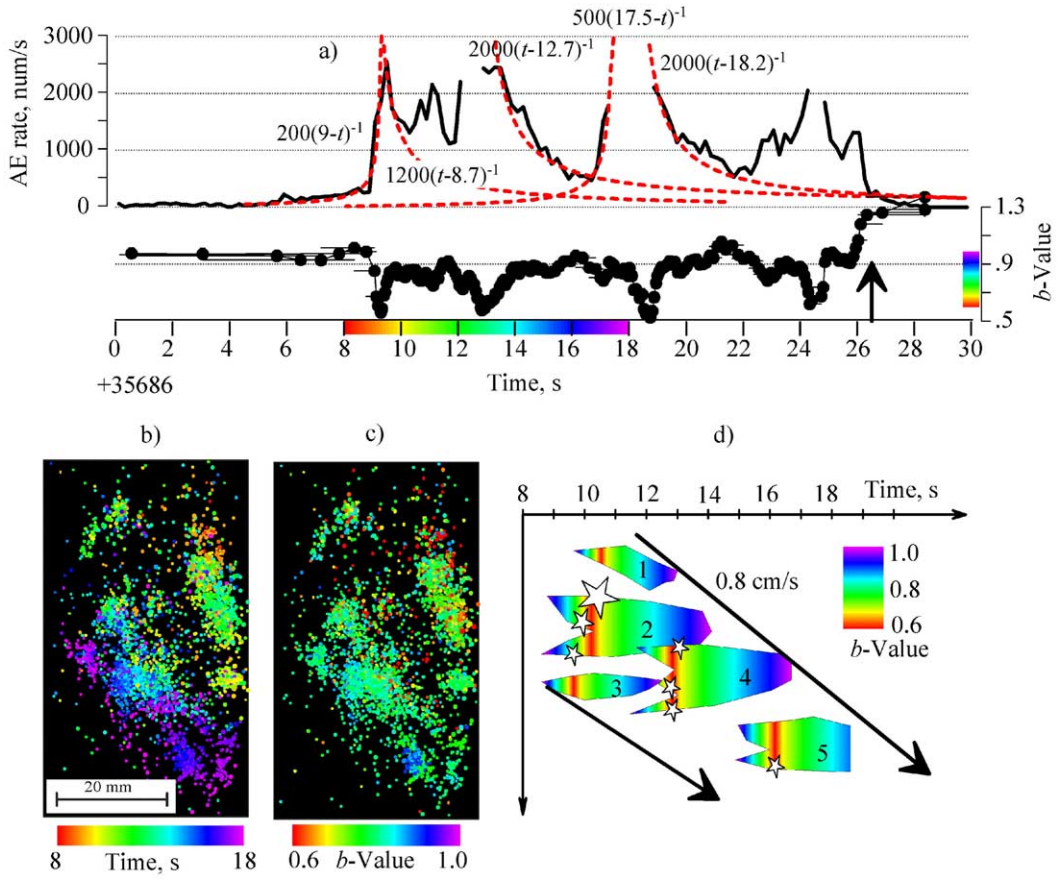

Fig. 2. (a) AE occurrence rates and *b*-values as functions of time from the initiation of faulting. AE rates were calculated at intervals of 0.2 s, and *b*-values were calculated by the maximum likelihood method for sets of 500 events with a running step of 125 events. (b,c) Distribution of hypocenters on the fault plane colored according to time and *b*-value. A *b*-value is assigned to each event according to its occurrence time using the *b*-value curve in panel a. (d) Schematic diagram showing the progressive fracture of coupled asperities resulting in a moving process zone (0.8 cm/s) based on the time–space distribution of AE hypocenters. Stars indicate the largest identified events.

individual asperities exhibit similar characteristics to the sequence of natural earthquakes. The fracturing of individual asperities is therefore treated in terms of foreshocks, the mainshock, and aftershocks in this paper.

As illustrated in Fig. 2, the first major asperity that fractured during this experiment was asperity 2. AE events associated with the fracture of this asperity can be readily identified because of the lack of overlap with the fracture of other asperities. Given this, asperity 2 is chosen as the main target for detailed analysis, although some data associated with other asperities are also used later. Fig. 3 shows the variation in *b*-values and relative magnitudes over time. A total of 2200 magnitude data were detected, and ~600 hypocenters were determined precisely. The *b*-values shown in Fig. 3 were calculated by the maximum likelihood method for sets of 100 events, with a running step of 25 events. A relatively small number of events was chosen specifically to examine the temporal variation in the *b*-value. The estimated error is 0.1–0.2 for *b*-values of 1.0–0.5. The short horizontal line at each data point indicates the time window used to calculate the corresponding *b*-value.

Fig. 4 shows the event number–magnitude relationships for some immediate foreshocks and

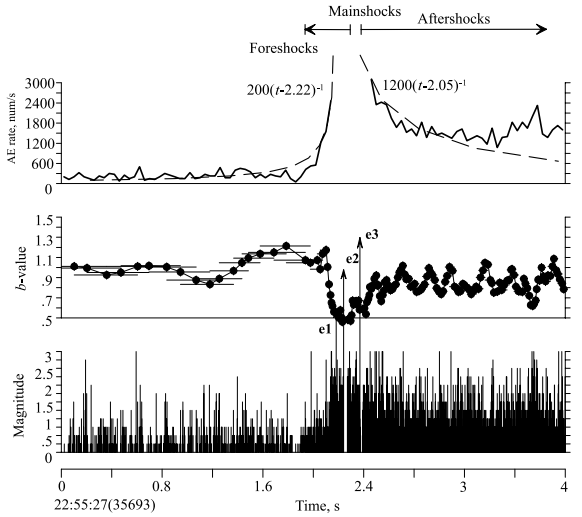

Fig. 3. AE rates, *b*-values, and AE event magnitudes associated with the fracture of asperity 2 in Fig. 1b. The *b*-values are calculated for sets of 100 events with a running step of 25 events by the maximum likelihood method. The magnitudes of the largest events e1, e2, and e3 were estimated from the continuation time of AE waves (Fig. 7). Dashed line denotes the power law of temporal distance from the mainshock. Note that the fitting is rough due to background AEs and overlap with subsequent fracture of other asperities.

aftershocks. The *b*-values estimated by the maximum likelihood method are also shown for comparison. In the magnitude plot, three large events labeled e1, e2 and e3 are indicated (Fig. 3b). These events released significantly greater energy than the events of average high magnitude. Fig. 5

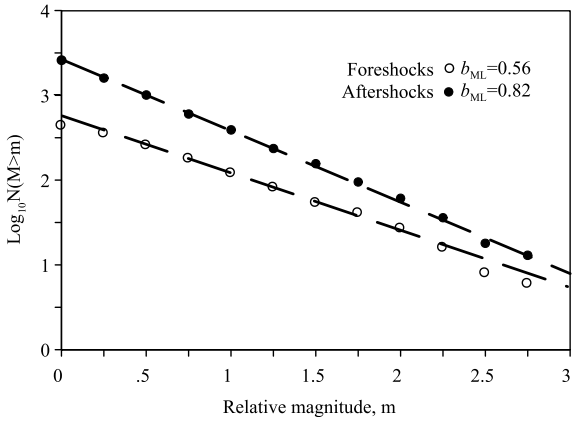

Fig. 4. Comparison of cumulative frequency–magnitude distributions of foreshocks with those of aftershocks indicated in Fig. 3.

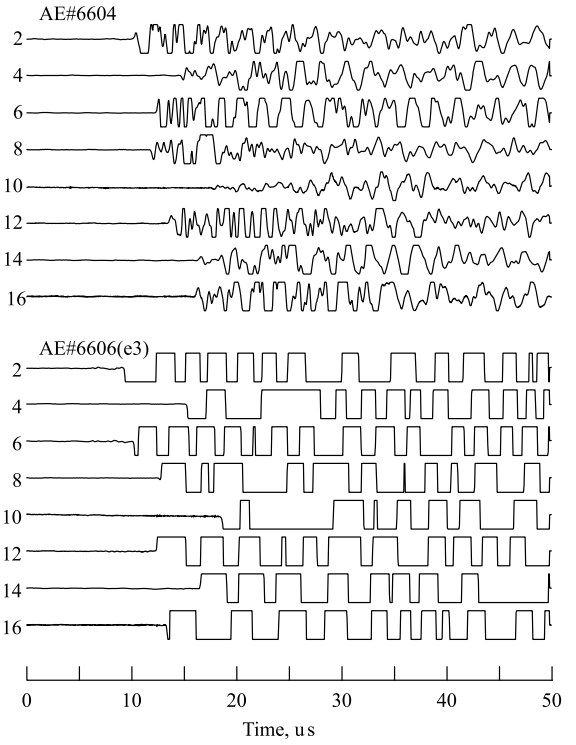

Fig. 5. Plots of waveforms for a normal event (AE#6604) and a mainshock (AE#6606). The larger amplitudes of mainshock waveforms saturate the recording system, and have a lower dominant frequency and coda several hundred times longer than the normal event.

is a comparison of the waveforms produced by such a normal event and the largest event e3. The dominant frequency of these large events is several times greater than that of the normal events. Another important feature of the mainshocks is the mechanism solution. The first-motion polarization data for e1 and e3 are plotted in Fig. 6a using an equal-area projection of the lower hemisphere of the focal sphere. The polarization distribution reflects a typical wing-crack, as illustrated in Fig. 6b, representing a shear crack with a tensile crack at one or both ends. Shear rupture of the shear crack and tensile opening of its wing(s) results in a non-double coupled focal mechanism. The shear plane estimated from the P-wave first motions (dashed line in Fig. 6a) is consistent with the fault plane (and therefore with the asperity plane). As these large events saturated the peak detector, the maximum ampli-

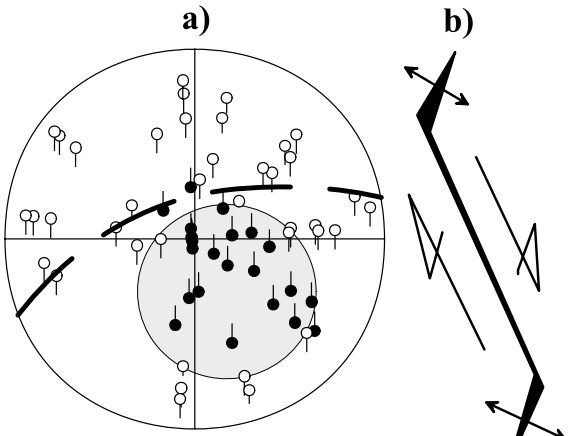

Fig. 6. (a) First-motion polarization data for two largest events (e1 and e3) plotted using an equal-area projection of the lower hemisphere of the focal sphere. (b) Typical wing-crack model indicated by the polarization distribution.

tudes are not available. However, the magnitudes can be roughly estimated from the wave continuation time. Fig. 7 shows the relationship between magnitudes and continuation times for some typical events. Similar to small earthquakes, these data can be fitted by a power law scaling given by $M = 3\log(T_D)+\text{const}$, where T_D is the continuation time in μs. Following this rule, the estimated relative magnitudes for e1, e2, and e3 are 4.25, 5.5, and 6.25, respectively. Therefore, e1 and e2 are treated as large foreshocks, and e3 is the mainshock. The AE data in Fig. 3 can then be treated as a foreshock–mainshock–aftershock sequence similar to natural earthquakes.

As shown in Fig. 7, typical events continue for 100–500 μs, whereas the largest events may be as long as 10–50 ms. The long tail of the largest events masked some following events, causing saturation of the event rates for those periods. Taking this into account, as shown in Fig. 2, the event rate for the foreshock and aftershock periods can be characterized by a simple law: the event rate R typically varies according to a power law as a function of the temporal distance $|t-t_M|$ to the main shock occurrence time t_M, as given by:

$$R = (c + |t-t_M|)^{-p} \quad (2)$$

with $p = 1$. For aftershocks, this law is well known as the modified Omori law [30,31], where c is a small constant and p is ~ 1 for most aftershock sequences. Recent studies have found there is a dissymmetry between the power laws of the foreshock and aftershock periods [32]. The parameters in the law are dominated by data for a short temporal distance from the mainshock. As the AE recording system used here saturates at an AE rate of greater than 5000 events per second, the parameters may have large uncertainty, particularly p. However, determination of the parameters is not the main goal of this paper. For simplicity, $p = 1$ is used to fit both foreshock and aftershocks periods as a rough approximation. It should be noted that foreshocks of later sequences were often initiated during the aftershock period of an earlier event, resulting in overlap. The b-value dropped from ~ 1.1 to ~ 0.5 in the foreshock period, and increased in the aftershock pe-

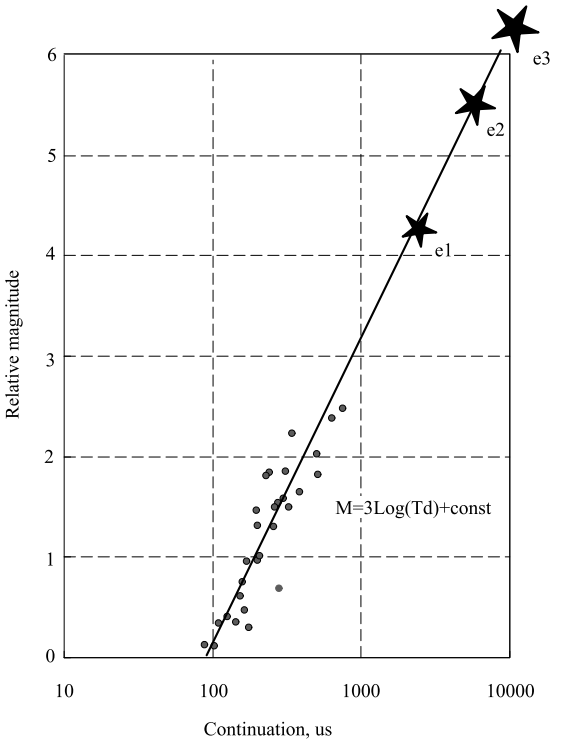

Fig. 7. Magnitude versus continuation time for typical AE events (circles). The magnitudes of the largest events (e1, e2, e3) were estimated based on the power law fitting (thick line).

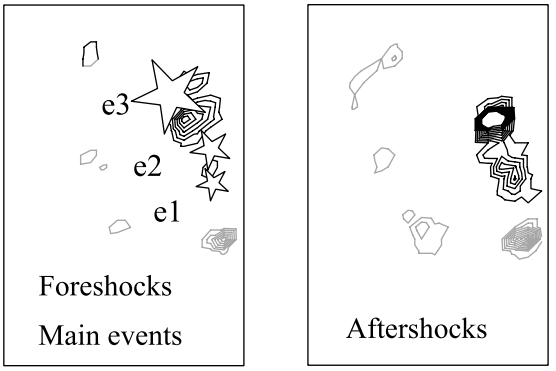

Fig. 8. Density maps of AE hypocenters associated with asperity 2. Stars indicate the three largest shocks (e1, e2, e3).

riod. On average, the *b*-value of immediate foreshocks (0.6) is smaller than that of aftershocks (0.82) (Fig. 4). This is in agreement with the widely observed rules for the sequence of natural earthquakes.

From the hypocenter density map near asperity 2 in Fig. 8, it is clear that the AE distribution associated with the fracture of a major asperity has several key features: foreshocks occurred mainly around the upper edge of the asperity, the mainshock and large foreshocks were located at the edge of the asperity (e1, e3) or near the foreshock front (e2), and aftershocks occurred throughout the entirety of the asperity, producing an inhomogeneous density distribution.

Fracture of the neighboring main asperity (asperity 4) started about 4 s after the mainshock of asperity 2. All asperities fractured one by one from top to bottom as illustrated in Fig. 2d, revealing movement of the process zone at a velocity of about 0.8 cm/s. This is presumably due to release of strain energy accumulated within an asperity during the mainshock, resulting in an enhancement of the stress concentration around the nearest neighboring intact asperity. The moving velocity of the process zone indicates the velocity of initial fault growth, or the quasi-static nucleation of shear faulting. The *b*-value exhibits a sharp minimum during the fracture of an individual asperity, corresponding to a complementary maximum in the AE event rate. Hence, the progressive fracture of multiple coupled asperities results in correlated short-term fluctuations in both *b*-value and AE event rate (Fig. 2a).

4. Discussion

The fracture process of several unbroken asperities on a shear fracture plane in a granitic porphyry is examined here in detail based on AE data. The test was carried out for one sample only due to the difficulty of finding two or more samples containing similar asperities. However, the experimental results are basically consistent with many other tests on samples containing a potential fracture plane of inhomogeneous strength distribution [19,20]. Overall, these tests demonstrate that the fracture process is strongly dependent on the structure of the fault plane, and basic features such as typical stages in the fracturing process can be seen. The fracture of an asperity is also dependent on the details of the asperity. The asperities in the present test are unbroken asperities surrounded by somewhat fractured (jointed) host rock. The results are also consistent with the current understanding of asperities based on seismic observations and numerical simulations. Therefore, the data obtained here associated with the fracture of such asperities are assumed to be typical.

4.1. *Variations in* b-*value and event rate in foreshock period*

For an individual sequence of foreshocks, the *b*-value drops from 1.0–1.2 to about 0.5 and the event rate increases with time according to a power law of the temporal distance from the mainshock, similar to the modified Omori law for aftershocks (Figs. 2 and 3). This result is in agreement with the theoretical model of subcritical crack growth [33–35], indicating that decreasing *b*-value reflects stress enhancement due to fracture growth in an asperity, particularly on its boundaries. A similar variation in the *b*-value has been pointed out for the foreshocks of natural earthquakes. For example, by comparing *b*-values for long-term seismicity and foreshocks occurring within hours and days of a mainshock, Molchan

et al. [36] found that the *b*-value drops by 0.5 during the foreshock period. However, this result and most other results on foreshocks represent a statistical average, and may not be characteristic of the behavior of individual foreshock sequences. Unfortunately, most large natural earthquakes are not preceded by a large number of identifiable foreshocks. To interpret this, the following two factors must be considered. One is the incompleteness of small earthquake records due to the magnitude threshold for detection. The other is that a well-developed natural fault might be quite homogeneous at small scales, particularly at seismogenic depths, and thus result in a low cutoff of magnitude. However, the lower limit of magnitude detection continues to improve through advances in observational techniques, and future work can be expected to reveal the importance of these factors.

Long-term foreshocks normally demonstrate a general increase in *b*-value, followed by an intermittent decrease and sharp decrease prior to fracture of a major asperity (see also [19,27]). This long-term tendency is also consistent with that observed before some large earthquakes, such as the M_w 7.8 Cape Kronotsky, Kamchatka, earthquake of 5 December 1997 [10] and the M_w 7.9 earthquake off Etorofu (Iturup), Kurile Islands, on 3 December 1995 [37], and volcanic eruptions (e.g. [38]).

4.2. *Variations in* b*-value and event rate in aftershock period*

Large earthquakes are typically followed by many aftershocks extending over days to months or even years. Enhanced observations after large earthquakes have revealed important information and greatly contributed to the understanding of aftershocks. It is well known that aftershocks are characterized by a high *b*-value and decreasing event rate according to the modified Omori law. After a large earthquake, the associated asperities can be mapped out by waveform inversion, and recent studies on seismic *b*-values have focused on the temporal–spatial variation in *b*-value and its relationship with asperities. For example, Hirose et al. [39] reported that a remarkable increase followed by a gradual decrease in *b*-value occurs after the rupture of asperities (mainshocks) off NE Japan based on analysis of a detailed earthquake catalogue. The experimental results presented in this paper are consistent with this finding. Mainshocks and aftershocks can therefore be considered to release stress accumulated at the associated asperity, thereby smoothing the strength distribution on the fault plane, resulting in a decrease in *b*-value.

4.3. *Migration of microcracking*

Das and Kostrov [15] described a numerical methodology for studying the fracture of a single asperity, and modeled a circular asperity embedded in a fractured infinite plane. Their calculation showed that the fracture first propagates along the edge of the asperity and then inward. The present experimental results are in general agreement with these numerical results, indicating that detailed microcracking data (or microseismic data in the case of natural earthquakes) are helpful for understanding the fracture process of asperities. However, in the experimental case, the presence of several asperities separated by distances smaller than the asperity dimensions, and the specific boundary condition at the end caps, may have been responsible for fault slip initiating at the upper end of the fault, with the result that subsequent fracture propagation proceeded downward with progressive fracturing of asperities.

4.4. *Mapping asperities*

The fracture of an individual asperity produces a dense cluster of microcracks with temporally varying *b*-values and event rates. Consequently, detailed time–space distributions of hypocenters, event rates and *b*-values may be constructed and used to identify asperities. Although asperities in the test samples were identified without the use of AE data, AE hypocenters in fact clustered in the region of asperities and could be used to map the asperities if necessary. If an asperity has been fractured, it is generally characterized as a low-*b* zone and a cluster of hypocenters, whereas if the asperity remains intact, it may exhibit a high

b-value and a low event rate. In either case, as suggested by Wiemer and Wyss [29] and Wyss et al. [40], the local recurrence time of large events can be used to map asperities more accurately.

4.5. Nucleation and hierarchical faulting process

In physical terms, seismic faulting must breaks parts of the healed fault before transitioning to quick propagation with fracturing of other healed segments. Thus, the rupture process may include the following experimentally observed stages: (1) a quasi-static nucleation at velocities on the order of cm/s, (2) quasi-dynamic growth at velocities on the order of $\sim$100 m/s, resulting in a weak initial phase that might be observable following improvement of techniques for earthquake observation such as stacked array data or borehole station data, and (3) dynamic propagation at velocities of 2–3 km/s producing strong motion. This nucleation model has been basically revealed through frictional tests using well-prepared fault planes (e.g. [41]). However, the experimental data presented in this paper demonstrate the new fact that a naturally healed fault containing unbroken asperities also exhibits a similar nucleation process to the fracture of well-prepared fault planes. A key factor in the nucleation model is the critical nucleation size, which controls the time from initiation to dynamic fracturing as well as precursory behaviors eventually applicable to earthquake prediction. A small critical nucleation size may result in short nucleation time and thus unpredictable dynamic faulting behavior, and vice versa. However, the nucleation procedure for natural earthquakes is still little understood due to the fact that the procedure has never been observed directly. Experimental studies in the laboratory are useful for elucidating the relationship between fault structure and the fracture process given the extreme difficulty inherent in observing natural tectonic earthquakes. From recent experimental studies, it can be suggested that the critical nucleation size of a given fault is controlled primarily by the strength distribution on the fault plane, and may differ from that estimated from the slip-weakening law and numerical simulation.

It is expected that the strength distribution of faults is globally somewhat self-similar, as suggested by the recognizable similarities between AE events at centimeter scales, microearthquakes at meter scales, and natural earthquakes at kilometer scales. However, for any given fault, the strength distribution may differ substantially from this self-similarity. Major asperities may exist at various scales and apparently control the seismogenic behavior of the fault. For instance, smaller long-lived isolated asperities in the creeping segment of the San Andreas fault are presumed to be the source of the repeating sequences of earthquakes [12,13]. The experimental results presented in this paper indicate that the quasi-static nucleation of the ultimate faulting is controlled by the asperities on the fault.

The fracture of an individual asperity exhibits a process similar to the sequence of natural earthquakes, where the foreshock period can be considered to correspond to the nucleation stage, and the mainshock to dynamic fracturing of the asperity. Hence, a hierarchical fracturing characteristic can be defined. The fracture of relative small asperities during the nucleation stage of large earthquakes would produce some foreshocks, which themselves will have associated fore-, main-, and aftershocks. This idea is shown schematically in Fig. 9. It is reasonable to presume that the stress accumulated at an asperity will be released by the mainshock to be redistributed among neighboring asperities. Therefore, mainshocks within coupled major asperities would occur sequentially, as observed experimentally, rather than simultaneously. If a fault contains multiple closely spaced asperities, the rupture process might involve fractures of all or a fraction of the total asperities. This could be happen at any stage between quasi-static rupture and dynamic rupture depending on the details of the asperity distribution.

It is important that the fracture of an asperity of any size generally contains a dynamic fracture phase, or mainshock. If an asperity fractured during the quasi-dynamic stage, it would contribute to the initial phases of the overall waveform, whereas if it fractured during the subsequent dynamic stage, it would play a role as a sub-event and affect the strong ground motion. If a fault is hierarchically heterogeneous at some scales, an

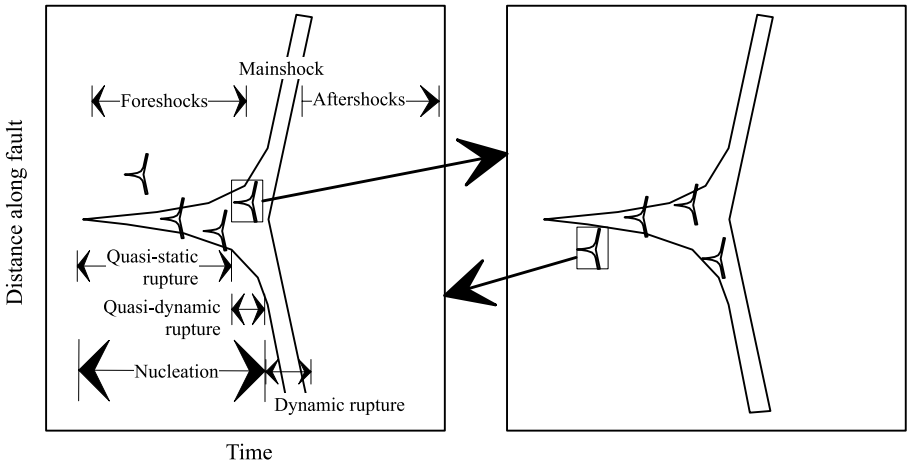

Fig. 9. Schematic diagram of hierarchical fracturing model for an inhomogeneous fault.

initial fracture process with noticeable precursory characteristics might be observed as a result of the progressive fracture of asperities at these scales. This kind of behavior may provide an opportunity for detecting the final preparation stages of large earthquakes, facilitating earthquake prediction. However, as mentioned above, the nucleation process of faulting depends strongly on the details of asperities on the fault plane. The structure of actual faults, particularly at earthquake source depth, is still very poorly understood and may be widely variable. Furthermore, at large scales, factors associated with rupture stop are important in the dynamic process of faulting. Even so, earthquakes of quite different magnitude may follow similar nucleation processes. Work linking laboratory experiments with seismic investigations based on earthquake observations are required to clarify these issues.

It should be noted that although seismology terminology has been used here to described the experimental results, the general conclusions are also applicable to other problems associated with the failure of rocks or rock masses, such as volcanic eruptions and rock bursts.

5. Conclusion

Based on AE measurements, the fracture process, particularly nucleation, of a shear fault containing several unbroken asperities in a granitic porphyry was examined in detail. AE data included 32-channel waveforms collected by a high-speed multi-channel waveform recording system, two-channel maximum amplitudes with a dynamic range of 55 dB, and two-channel waveforms with 16-bit dynamic range and sample lengths of up to 1 s. AE hypocenters and relative magnitudes were determined based on these measurements.

Quasi-static nucleation of shear faulting was found to correspond to the fracture of coupled asperities on the fault plan. The fracture of individual asperities occurs in three distinct stages. In the first stage, the event rate increases and *b*-value decreases (from $\sim$1.1 to $\sim$0.5), with events initiated at the edge of the asperity. The second stage is a short period in which one or a few very large events begin at the edge of the asperity or the front of hypocenters in the first stage. The third stage is characterized by a remarkable increase and subsequent gradual decrease in *b*-value with a decreasing event rate. Event rates in the first and third stages obey the modified Omori law for natural earthquakes. These facts demonstrate that AEs caused by the fracture of asperities have similar characteristics to the sequence of natural earthquakes, consisting of foreshocks, the mainshock, and aftershocks.

The fracture of neighboring asperities was found to be initiated after the mainshock of a

particular asperity. This is presumably because strain energy accumulated within an asperity is released by the mainshock and redistributed as enhanced stress concentration around the nearest neighboring intact asperities. The progressive fracturing of multiple, coupled asperities during the nucleation of shear faulting results in short-term precursory fluctuations in both the *b*-value and event rate. The present experimental results are consistent with recent findings for natural earthquakes based on improved observations, demonstrating that laboratory studies under well-controlled conditions using well-prepared samples containing well-known asperities can be expected to be useful for understanding the physics of rupturing, particularly for the poorly understood final preparation stage of large earthquakes.

Acknowledgements

Thanks are extended to Ian Main and Didier Sornette for helpful suggestions and critical comments for improving the manuscript. This work was supported in part by the Chinese Ministry of Science and Technology under 2001BA601B02, and AIST, Japan.*[VC]*

References

[1] H. Kanamori, G.S. Stewart, Seismological asperity earthquake of February 4, 1976, J. Geophys. Res. 83 (1978) 3427–3434.
[2] K. Aki, Characterization of barriers on an earthquake fault, J. Geophys. Res. 84 (1979) 6140–6148.
[3] K. Aki, Asperities, barriers, characteristic earthquake and strong motion prediction, J. Geophys. Res. 89 (1984) 5867–5872.
[4] S.H. Hartzel, T.H. Heaton, Inversion of strong ground motion and teleseismic waveform data for the fault rupture history of the 1979 Imperial Valley, California, earthquake, Bull. Seismol. Soc. Am. 73 (1983) 1553–1583.
[5] A. Pinar, Source inversion of the October 1, 1995, Dina earthquake (Ms = 6.1): a rupture model with implications for seismotectonics in SW Turkey, Tectonophysics 292 (1998) 255–266.
[6] Y. Zeng, C.-H. Chen, Fault rupture process of the 20 September 1999 Chi-Chi, Taiwan, earthquake, Bull. Seismol. Soc. Am. 91 (2001) 1088–1098.
[7] S. Ide, Complex source processes and the interaction of moderate earthquakes during the earthquake swarm in the Hida-Mountains, Japan, 1998, Tectonophysics 334 (2001) 35–54.
[8] T. Okada, N. Umino, Y. Ito, T. Matsuzawa, A. Hasegawa, M. Kamiyama, Source processes of 15 september 1998 M 5.0 Sendai, Northeastern Japan, earthquake and its M 3.8 foreshock by waveform inversion, Bull. Seismol. Soc. Am. 91 (2001) 1607–1618.
[9] M. Wyss, S. Matsumura, Most likely locations of large earthquakes in the Kanto and Tokai areas, Japan, based on the local recurrence times, Phys. Earth Planet. Inter.s 131 (2002) 173–184.
[10] F.R. Zuniga, M. Wyss, Most- and least-likely locations of large to great earthquakes along the Pacific coast of Mexico estimated from local recurrence time based on b-values, Bull. Seismol. Soc. Am. 91 (2001) 1717–1728.
[11] V.M. Zobin, V.I. Levina, The rupture process of the Mw 7.8 Cape Kronotsky, Kamchatka, earthquake of 5 December 1997 and its relationship to foreshocks and aftershocks, Bull. Seismol. Soc. Am. 91 (2001) 1619–1628.
[12] R.M. Nadeau, L.R. Johnson, Seismological studies at Parkfield VI: Moment release rate and estimates of source parameters for small repeating earthquakes, Bull. Seismol. Soc. Am. 88 (1998) 790–814.
[13] C.G. Sammis, R.M. Nadeau, L.R. Johnson, How strong is an asperity?, J. Geophys. Res. 104 (1999) 10609–10619.
[14] C.G. Sammis, J.R. Rice, Repeating earthquakes as low-drop events at a border between locked and creeping fault patches, Bull. Seismol. Soc. Am. 91 (2001) 532–537.
[15] S. Das, B.V. Kostrov, Breaking of a single asperity: rupture process and seismic radiation, J. Geophys. Res. 88 (1983) 4277–4288.
[16] D.A. Lockner, J.D. Byerlee, V. Kuksenko, A. Ponomarev, A. Sidorin, Quasi-static fault growth and shear fracture energy in granite, Nature 350 (1991) 39–42.
[17] X.-L. Lei, K. Kusunose, M.V.M.S. Rao, O. Nishizawa, T. Satoh, Quasi-static fault growth and cracking in homogeneous brittle rock under triaxial compression using acoustic emission monitoring, J. Geophys. Res. 105 (2000) 6127–6139.
[18] A. Zang, F.C. Wagner, S. Stanchits, C. Janssen, G. Dresen, Fracture process zone in granite, J. Geophys. Res. 105 (2000) 23651–23661.
[19] X.-L. Lei, K. Kusunose, O. Nishizawa, A. Cho, T. Satoh, On the spatio-temporal distribution of acoustic emission in two granitic rocks under triaxial compression: the role of pre-existing cracks, Geophys. Res. Lett. 27 (2000) 1997–2000.
[20] X.-L. Lei, O. Nishizawa, K. Kusunose, A. Cho, T. Satoh, On the compressive failure of shale samples containing quartz-healed joints using rapid AE monitoring: the role of asperities, Tectonophysics 328 (2000) 329–340.
[21] T. Hirata, Fractyal dimension of fault system in Japan: Fracture structure in rock fracture geometry at various scales, Pure Appl. Geophys. 131 (1989) 157–170.
[22] G. Ouillon, D. Sornette, C. Castaing, Organization of joints and faults for 1 cm to 100 km scales revealed by

optimized anisotropy wavelet coefficient method and multifractal analysis, Nonlinear Process. Geophys. 2 (1995) 158–177.
[23] E. Bonnet, O. Bour, N.E. Odling, P. Davy, I. Main, P. Cowie, B. Berkowitz, Scaling of fracture systems in geological media, Rev. Geophys. 39 (2001) 347–383.
[24] C.H. Scholz, The frequency-magnitude relation of microcracking in rock and its relation to earthquakes, Bull. Seismol. Soc. Am. 58 (1968) 399–415.
[25] N. Kato, K. Yamamoto, T. Hirasawa, Microfracture processes in the break down zone during dynamic shear rupture inferred from laboratory observation of near-fault high-frequency strong motion, Pure Appl. Geophys. 142 (1994) 713–734.
[26] X.-L. Lei, O. Nishizawa, K. Kusunose, Band-limited heterogeneous fractal structure of earthquakes and acoustic emission events, Geophys. J. Int. 115 (1993) 79–84.
[27] X.-L. Lei, K. Kusunose, T. Satoh, O. Nishizawa, The hierarchical rupture process of a fault: an experimental study, Phys. Earth Planet. Inter. 137 (2003) 213–228.
[28] X.-L. Lei, O. Nishizawa, K. Kusunose, T. Satoh, Fractal structure of the hypocenter distribution and focal mechanism solutions of AE in two granites of different grain size, J. Phys. Earth 40 (1992) 617–634.
[29] S. Wiemer, M. Wyss, Mapping the frequency-magnitude distribution in asperities: An improved technique to calculate recurrence times?, J. Geophys. Res. 102 (1997) 15115–15128.
[30] F. Omori, On the aftershocks of earthquakes, J. Coll. Sci. Imp. Univ. Tokyo 7 (1894) 111–200.
[31] T. Utsu, Y. Ogata, R.S. Matsu'ura, The centenary of the Omori formula for a decay law of aftershock activity, J. Phys. Earth 43 (1995) 1–33.
[32] A. Helmstetter, D. Sornette, J.-R. Grasso, Mainshocks are aftershocks of conditional foreshocks: how do foreshock statistical properties emerge from aftershock laws? J. Geophys. Res. 108 (B10) (2003) 10.1029/20002JB001991.
[33] I.G. Main, P.G. Meredith, C. Jones, A reinterpretation of the precursory seismic *b*-value anomaly using fracture mechanics, Geophys. J. 96 (1989) 131–138.
[34] I.G. Main, P.G. Meredith, P.R. Sammonds, Temporal variations in seismic event rate and *b*-values from stress corrosion constitutive laws, Tectonophysics 211 (1992) 233–246.
[35] I.G. Main, P.R. Sammonds, P.G. Meredith, Application of a modified Griffith criterion to the evolution of fractal damage during compressional rock failure, Geophys. J. Int. 115 (1993) 367–380.
[36] G.M. Molchan, T.L. Kronrod, A.K. Nekrasova, Immediate foreshocks: time variation of the *b*-value, Phys. Earth Planet. Inter. 111 (1999) 229–240.
[37] N. Hurukawa, The 1995 off-Etorofu earthquake: joint relocation of foreshocks, the mainshock, and aftershock and implications for the earthquake nucleation process, Bull. Seismol. Soc. Am. 88 (1998) 1112–1126.
[38] S. Vinciguerra, Seismic scaling exponents as a tool in detecting stress corrosion crack growth leading to the September-October 1989 flank eruption at Mt. Etna volcano, Geophys. Res. Lett. 26 (1999) 3689–3692.
[39] F. Hirose, A. Nakamura, A. Hasegawam, *b*-value variation associated with the rupture of asperities – spatial and temporal distributions of b-value East off NE Japan, Zisin 53 (2002) 249–260.
[40] M. Wyss, D. Schorlemmer, S. Wiemer, Mapping asperity by minima of local recurrence time: the San Jacinto-Elsinore fault zones, J. Geophys. Res. 105 (2000) 7829–7844.
[41] M. Ohnaka, A physical scaling relation between the size of an earthquake and its nucleation zone size, PAGEOPH 157 (2000) 2259–2282.